ACS OMEGA

Article

http://pubs.acs.org/journal/acsodf

Assessing the Ability of Spectroscopic Methods to Determine the Difference in the Folding Propensities of Highly Similar β-Hairpins

Hanna Andersson,[†] Emma Danelius,[†] Patrik Jarvoll,[†] Stephan Niebling,[†,§] Ashley J. Hughes,[†] Sebastian Westenhoff,[†] Ulrika Brath,[†,∥] and Máté Erdélyi*[,†,‡]

[†]Department of Chemistry and Molecular Biology, University of Gothenburg, Kemivägen 10, SE-412 96 Gothenburg, Sweden

[‡]The Swedish NMR Centre, Medicinaregatan 5c, SE-413 96 Gothenburg, Sweden

Supporting Information

ABSTRACT: We have evaluated the ability of nuclear magnetic resonance (NMR) and circular dichroism (CD) spectroscopies to describe the difference in the folding propensities of two structurally highly similar cyclic β-hairpins, comparing the outcome to that of molecular dynamics simulations. NAMFIS-type NMR ensemble analysis and CD spectroscopy were observed to accurately describe the consequence of altering a single interaction site, whereas a single-site ^{13}C NMR chemical shift melting curve-based technique was not.

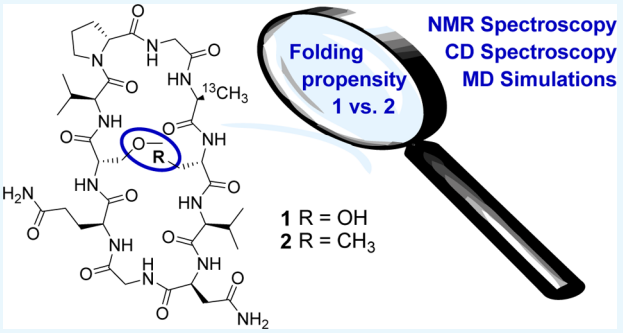

1. INTRODUCTION

Peptides,[1−3] β-hairpins in particular,[4−8] are common model systems for the investigation of weak interactions that direct protein folding. Peptide conformational equilibria in solution is typically evaluated using nuclear magnetic resonance (NMR), circular dichroism (CD), infrared (IR) spectroscopy, differential scanning calorimetry, or by computational analysis.[5,7] Many experimental studies apply one of the above techniques,[6,9−15] whereas the ability of the methods to describe peptide folding has scarcely been compared; nor has their ability to detect a slight difference in folding upon a minor structural change of a peptide been assessed. Such a comparative evaluation is expected to help the method of selection for future studies and to provide a basis for comparison of data for systems whose folding was described using different techniques.

2. RESULTS AND DISCUSSION

To evaluate the ability of the NMR-based ensemble analysis technique NAMFIS,[16] of chemical shift melting curve analysis and of CD spectroscopy for detecting the influence of a small structural modification on β-hairpin folding, we have synthesized[17] cyclic decapeptides **1** and **2** (Figure 1). These peptides differ only in the availability or absence of a hydrogen bond donor site, permitting or preventing the formation of an interstrand hydrogen bond, stabilizing the β-hairpin.[18] Molecular dynamics (MD) simulation was used as an independent, nonspectroscopic method in the benchmarking of the spectroscopic techniques, suggesting 64% folded β-hairpin population for **1** and 43% for **2** in dimethyl sulfoxide (DMSO) at 298 K. Here, following a previously established protocol,[19]

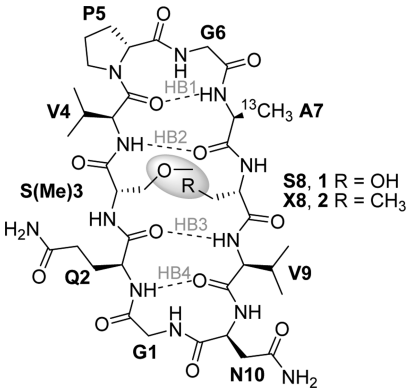

Figure 1. Structures of β-hairpin peptides **1** and **2**, with the interaction center encircled and highlighted in gray. The possible interstrand hydrogen bonds are denoted as HB1−HB4.

conformations possessing ≥3 interstrand hydrogen bonds HB1−4 (Figure 1) in the MD trajectory frames were defined as folded (Table S20). The phi (φ) and psi (ψ) dihedral angles of the ^{D}P5−G6 turn of folded **1** and **2** indicated it to form a type II′ β-turn (Figure S16), whereas those of the N10−G1 turn segment to adopt a type II β-turn (Figure S17).[20,21] In agreement with the expected formation of an interstrand S(Me)3−S8 hydrogen bond in **1**, the bond lengths of HB2 and HB3 were observed to be shorter in **1** compared with those of

Received: December 8, 2016
Accepted: January 16, 2017
Published: February 13, 2017

DOI: 10.1021/acsomega.6b00484
ACS Omega 2017, 2, 508−516

2, whereas their turn regions showed comparable HB1 and HB4 distances (Figure S15).

Population change maps (Tables S21 and S22), generated by following the transitions between various hydrogen-bonded states in the MD trajectory frames, revealed that both peptides fold by first forming the HB4 hydrogen bond, followed by HB1, and finally HB3 and HB2, as shown in Figure 2.

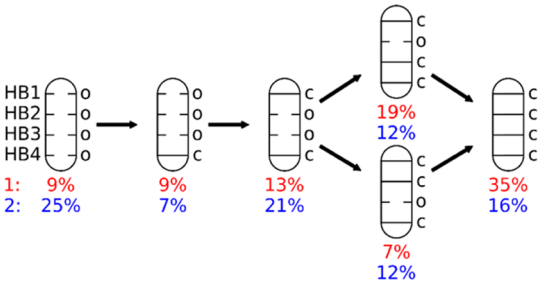

Figure 2. Folding pathways and populations for peptides **1** (red) and **2** (blue). The most probable folding route from the fully unfolded *oooo* to the completely folded *cccc* conformation was derived from the population change maps that are shown in Tables S21 and S22. The probability of each state at room temperature is denoted below the hydrogen bond schemes, with red and blue indicating **1** and **2**, respectively. Probabilities of the less populated states are given in the Supporting Information.

CD spectroscopy is a widely used tool for the characterization of the overall secondary structure of proteins and peptides and is commonly performed by deconvolution of the spectra into various secondary structure components.[12,22] The spectra of the two peptides (Figure 3) are remarkably different.

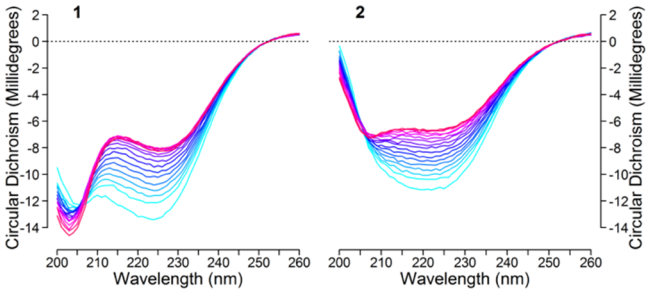

Figure 3. Concentration-corrected CD data obtained for **1** and **2** acquired in the 262−342 K interval for acetonitrile solutions ($c \approx 44$ μM, $b = 2$ mm) indicate that both peptides adopt a twisted antiparallel β-hairpin conformation, with a strongly temperature-dependent negative band at 216−220 nm, permitting a detailed thermodynamic analysis of folding. The OH to CH_3 substitution causes a significant change in the CD spectra.

In accordance with the literature, **1** shows a double minimum at 205 and 223 nm, which is indicative of β-hairpin possessing a strong type II′ β-turn.[23] By contrast, **2**, expected to exhibit a lower β-hairpin content than **1**, shows a broad minimum at 220 nm, characteristic for β-hairpins.[23] Accordingly, **1** shows a stronger negative molar ellipticity in the 216−220 nm interval than **2**, which may reflect a higher stability of its folded structure. However, these CD features are not directly interpretable as quantitative indicators for relative folding propensity. For the estimation of the folded population of **1** and **2**, we have obtained the CD spectra within an 80 K temperature interval at λ = 200−260 nm (Figure 3) and have deconvoluted the spectra into predominantly β-hairpin and random coil components via principal component analysis (PCA) (Figure S24).[12] With increasing temperature, the broad negative CD band at 216−220 nm, corresponding to the β-hairpin structure[24] of both **1** and **2**, loses intensity, whereas the band at 200 nm, consistent with a random coil component, gains intensity (Figure 3). The strong negative CD bands at 205 and 223 nm, observed for **1**, qualitatively resembles the CD spectra of the β-hairpins encompassing a type II′ β-turn described by Gibbs et al. (Figure S25).[23] The isodichroic point observed at 207 nm is indicative of a two-state system present in both peptides. Tracking the ellipticity at 216 nm indicates that **1** has a 13% more folded β-hairpin structure relative to **2**. PCA (Figure 4), enabling a direct comparison of the unfolding

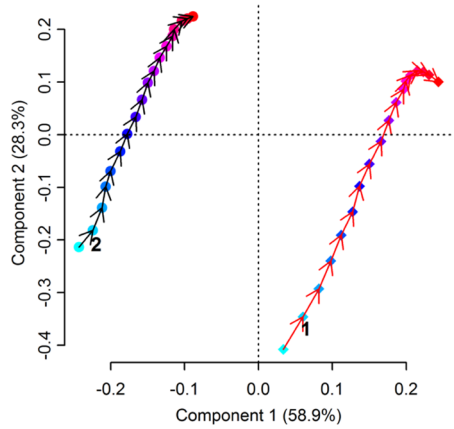

Figure 4. PCA of the CD data of **1** (diamonds) and **2** (circles) undergoing thermal unfolding from 262 to 342 K in 19 steps, color-coded from cyan to red. The two main components, that is, the random coil (component **1**) and the β-hairpin (component **2**), represent 87.2% of the observable variance. At high temperatures, the thermal unfolding of **1** reaches a plateau with no further loss of the β-turn element, whereas that of **2** continues to lose the β-turn content, suggesting a more stable β-hairpin conformation for **1** compared with that for **2**.

pathways of the two peptides, shows that upon increasing the temperature, the proportion of the random coil structure increases, as reflected by an increase in component **1** (Figure 4), whereas that of β-turn decreases, as reflected by an increase in component **2**, for both peptides. At high temperatures, the thermal unfolding of **1** reaches a plateau with no further loss of the β-turn element, suggesting a more stable folded structure for **1** compared with **2**. The latter continues to increase in component **2** and thus losing β-turn even at high temperatures. Overall, PCA indicates a more stable folded structure for **1** than **2**.

Whereas the computational (vide supra) and NMR spectroscopic (vide infra) analyses were performed in DMSO, because of the lack of transparency of DMSO in the wavelength interval typical of amide absorptions, the CD spectra were acquired in acetonitrile. As both solvents are polar aprotic and have similar polarity indices (DMSO, 7.2 and CH_3CN, 5.8), this solvent alteration was expected to not have any major influence on the folding of the studied systems. Accordingly, the conclusions drawn from the CD spectroscopic analysis are in good agreement with those of the MD and NAMFIS-based NMR analyses. Hence, CD spectroscopy is capable of detecting the stability difference between two structurally highly similar

DOI: 10.1021/acsomega.6b00484
ACS Omega 2017, 2, 508−516

peptides. The different solvents used for CD as compared with MD and NMR may, however, partially explain the slight variation in the difference in the folding of **1** and **2**, as observed using different techniques.

In contrast to CD spectroscopy that gives one overall signal for a studied solution, NMR spectroscopy provides detailed, atomic-level information on the molecular structure. Peptide folding can be assessed both qualitatively and quantitatively using ^{1}H and ^{13}C NMR chemical shifts. $^{13}C\beta$ and $^{13}C\alpha$ structuring shifts, for example, which are defined as chemical shift deviations (CSDs) from random coil values, are frequently used for identifying and evaluating β-hairpin folding.[13,25−28] The qualitative CSD analysis of **1** and **2** (see the Experimental Section and Supporting Information for details) indicates β-hairpin conformation for both model peptides (Tables S6 and S7, and Figures S3 and S4). However, because the reference shifts (i.e., $\delta_{\text{random coil}}$ and $\text{CSD}_{100\%\text{ folded}}$) that are available in the literature are for aqueous solutions and/or for vastly different sequences, they are not fully applicable to **1** and **2**. For a quantitative assessment of the β-hairpin population from structuring shifts (i.e., $\text{CSD}_{\text{obs}}/\text{CSD}_{100\%\text{ folded}}$), comparison with reference values obtained for suitable control peptides under identical experimental conditions would be needed.

Nuclear Overhauser effects (NOEs) and *J*-couplings are most commonly used to calculate interatomic distances and dihedral angles, to describe peptide conformations. As these are population-averaged observables,[29] for the proper description of the structure of flexible molecules, these have to be deconvoluted into the population-weighted contributions of the NOEs and *J*-couplings of individual conformations available in solution. Molecular ensembles of, for example, peptides,[18,29−31] macrocycles,[32−34] and drug candidates[35] have been successfully identified by deconvolution of their time-averaged NMR data using the NAMFIS algorithm (for a detailed description of the method, see ref 29). It uses a computationally generated theoretical conformational pool, which covers the entire conformational space available for a flexible molecule, and experimentally observed time averaged structural parameters. The latter are used for the identification of conformers present in the solution and for the calculation of their probabilities corresponding to their molecular fractions. Theoretical ensembles for **1** and **2** were predicted in this study using Monte Carlo conformational search with intermediate torsion sampling, followed by molecular mechanics energy minimization, as implemented in the software Macromodel (v.9.1).[36] To ensure full coverage of the conformational space, theoretical conformational ensembles were generated using two different force fields, (OPLS)-2005 and Amber* (developed for peptides). The conformations within 42 kJ/mol from the global minimum were combined (Table S13), and redundant conformations were eliminated using the clustering analysis using a 2.5 Å root-mean-square deviation (RMSD) cutoff for all heavy atom coordinates. These conformational pools containing 80 and 147 conformations for **1** and **2**, respectively, were used as theoretical inputs for the NAMFIS calculations. Using experimental NOE-based distance and *J*-based dihedral angle data (overall 36 vs 39 restraints for **1** and **2**, respectively, as given in Tables S15 and S16), NAMFIS[29] identified 9 versus 11 solution conformations and computed their molar fractions. Out of these ensembles, 58% versus 29% were folded β-hairpins for **1** and **2** (Table S14), respectively, indicating a 29 percentage point increased folding of the peptide capable of forming an interstrand sidechain-to-sidechain hydrogen bond. This hydrogen bond, between S8 and S(Me)3, was present in 58% probability in the conformational ensemble, identified on the basis of experimental NMR restraints. The folded conformations of **1** and **2** are shown in Figure 5 and are

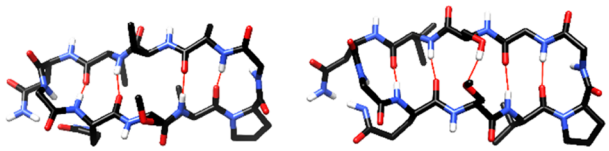

Figure 5. Folded conformations of peptides **1** (right) and **2** (left), identified by the NAMFIS algorithm based on an NOE and *J*-based selection from a theoretical pool of conformations generated by a restraint-free Monte Carlo conformational search algorithm. The interstrand S8−S(Me)3 hydrogen bond was present in 58% of the conformations of the ensemble for **1**, whereas its formation is prevented for **2**.

apart from the presence or absence of the interchain hydrogen bond between S8 and S(Me)3 highly similar. The full conformational ensembles are depicted in Figures S10 and S11, with the population of the individual solution conformers being given in Table S14. The NOE- and *J*-based ensemble analyses were validated using standard methods, that is, through evaluation of the reliability of the conformational restraints by the addition of 10% random noise to the experimental data, by the random removal of individual restraints, and by comparison of the experimentally observed and back-calculated distances and scalar coupling constants as given in Tables S15 and S16.

Studying the temperature dependence of NMR chemical shifts is another common approach for quantitating the extent of folding. Signal overlaps and small chemical shift changes over the available temperature range, yielding an incomplete melting curve, prohibited a detailed analysis of the ^{1}H NMR data of **1** and **2**. Upon ^{13}C-labeling of the A7 methyl group (Figure 1), an amino acid positioned next to the S8−S(Me)3 interaction site and thus used as a reporter nucleus, we obtained temperature-dependent ^{13}C NMR data for **1** and **2** (Figure 6 and Table S8) and performed thermodynamic analyses, following the literature procedure of Honda et al.[37,38] Analogous to previous studies, shallow partial thermal transition curves were observed and were analyzed using a two-state folding model with a nonlinear least-squares curve-fitting procedure (see the

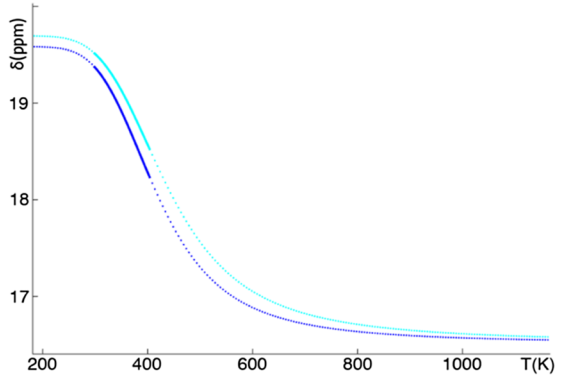

Figure 6. Best fitted curves of variable temperature (VT) ^{13}C NMR data for A7−$^{13}C\beta$ in **1** (blue) and **2** (cyan) to eq 1 (Supporting Information). The NMR data were acquired at 299−404 K in the DMSO-d_6 solution.

DOI: 10.1021/acsomega.6b00484
ACS Omega 2017, 2, 508−516

Experimental Section and Supporting Information for details).[37,38]

For the estimation of the relative thermodynamic stability of the peptides, the ratio of their unfolding constants, K_U^{P1}/K_U^{P2}, is determined using eq 1.

$$K_U(\delta_U^{P1} - \delta_{obs}^{P1})(\delta_{obs}^{P2} - \delta_F^{P2}) = (\delta_{obs}^{P1} - \delta_F^{P1})(\delta_U^{P2} - \delta_{obs}^{P2}) \quad (1)$$

In eq 1, δ_U and δ_F are the chemical shifts of the completely unfolded and the fully folded states of the peptide, respectively, whereas δ_{obs} is the observed chemical shift at a given temperature and K_U is the ratio of the unfolding constants of **1** and **2**, which are denoted as P1 and P2. Importantly, the slope of the plot $(\delta_U^{P1} - \delta_{obs}^{P1})(\delta_{obs}^{P2} - \delta_F^{P2})$ versus $(\delta_{obs}^{P1} - \delta_F^{P1})(\delta_U^{P2} - \delta_{obs}^{P2})$ (Figure 7) quantifies the relative stability, here the ratio

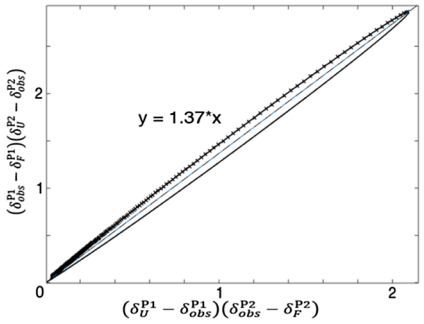

Figure 7. Unfolding ratio of **1** and **2**, determined using eq 1 from the VT ^{13}C NMR measurements acquiring the chemical shift of A7–$^{13}C\beta$.

of the unfolding constants of **1** and **2**. Hence, a slope greater than 1 indicates a higher stability of **2** compared with that of **1**. The plot is nonlinear because of the difference in the folding enthalpy of the studied systems; yet, its slope can be easily determined. As eq 1 includes chemical shifts only, we acquired the ^{13}C NMR shift of A7–$^{13}C\beta$ of **1** and **2** simultaneously in the same solution, which maximizes the accuracy of the data by minimizing referencing errors and errors due to differences in the sample temperature. The obtained slope indicates a 37% higher stability of **2** compared with that of **1**, which is in disagreement with the MD, CD, and NOE/*J*-based analyses. Analysis of the CD data using the method of Honda et al.[38] indicates an 8% higher folded population for **1** compared with that for **2**. Following the literature,[15] here we analyzed folding by following the temperature dependence of the chemical shift of a single reporter nucleus. The data of one selected nucleus, however, may better reflect local than overall conformational changes. This presumption was corroborated by a modified NAMFIS analysis including only the NOE data of A7, which also suggested a higher folded population for **2** compared with that of **1** (Tables S17–S19 and Figures S12 and S13). The latter analysis indicates that great care needs to be taken when interpreting the data of a single nucleus in a peptide or protein sequence. With access to an 800 MHz spectrometer equipped with a cryogenic probe with a cooled ^{13}C preamplifier, and thus to supreme ^{13}C NMR sensitivity, we acquired the ^{13}C NMR shifts of all unlabeled positions of the peptides in the temperature range of 296–343 K (Figures S5–S7). This narrower temperature range, limited by the hardware, unfortunately did not permit the acquisition of sufficiently large amounts of data for a reliable thermodynamic analysis (Figures S22 and S23). No chemical shift changes larger than those observed for the reporter nucleus of A7 were detected for the α- and β-carbons of the unlabeled amino acids.

3. CONCLUSIONS

Overall, the CD and NAMFIS analyses reliably reproduced the MD-predicted higher stability of **1** compared with that of **2** and thus were shown to be applicable for the detection of changes in the β-hairpin stability upon a minor structural alteration. Thermodynamic analysis of the temperature-dependent variation in the ^{13}C NMR chemical shift of a single reporter nucleus, however, suggested an opposite trend of stability. Whereas the CD and NOE/*J*-based methods include data reflecting the overall conformation, the latter chemical shift analysis reports only the changes experienced by one atom in the peptides and thus predominantly may reflect changes in the local environment. Our results suggest that great care has to be taken when selecting the method for the analysis of differences in the peptide of closely related structures. Preferably, the outcome of several complementary techniques should be compared, and techniques reporting the data for only single amino acids should be avoided.

4. EXPERIMENTAL SECTION

4.1. Peptide Synthesis. *4.1.1. General Information.* Solid-phase peptide synthesis (SPPS) was performed using an automated benchtop peptide synthesizer. Analytical reversed-phase high-performance liquid chromatography (RP-HPLC)–mass spectrometry (MS) was performed on a system with a single quadrupole mass spectrometer (ESI^+ or ESI^-) and a single wavelength UV detector (270 nm), using a C8-EC column (120 Å, 4 μm, 4.6 × 50 mm) with gradients of CH_3CN/H_2O (0.1% HCOOH) at a flow rate of 1 mL/min. Preparative RP-HPLC was performed on a system with a single wavelength UV detector (220 nm), using a C18 column (110 Å, 10 μm, 21.2 × 250 mm) at a flow rate of 20 mL/min, with gradients of CH_3CN/H_2O (0.1% HCOOH). Analytical RP-HPLC was performed on a system with a single wavelength UV detector (220 or 230 nm), using a C18 column (110 Å, 5 μm, 3.2 × 250 mm) at a flow rate of 1 mL/min or a C18 column (100 Å, 3 μm, 4.6 × 50 mm) at a flow rate of 2.5 mL/min, with gradients of CH_3CN/H_2O (0.1% HCOOH). High-resolution MS analyses [Q-time-of-flight (TOF)-MS] were performed at Stenhagen Analyslab AB, Gothenburg, Sweden. All chemicals were purchased from commercial sources and used without further purification.

4.1.2. General Procedure for Peptide Synthesis and Purification. The linear peptide sequences were synthesized on a 300 μmol scale following the standard Nα-Fmoc protecting group strategy[39] (Scheme S1). Before the initial coupling, the resin was swollen in dimethylformamide (DMF) for 3 × 10 min. A mixture of the appropriate amino acid (2 equiv), TBTU (*N*,*N*,*N*′,*N*′-tetramethyl-O-(benzotriazol-1-yl)-uronium tetrafluoroborate) (2 equiv), and N,N-diisopropylethylamine (DIPEA, 4 equiv) in DMF was added to the resin, and the reaction mixture was agitated by nitrogen bubbling. For Fmoc-[3-^{13}C]Ala-OH, the number of equivalents was reduced to 1.3. Double couplings were used for all amino acids (2 × 1.5 h for Fmoc-D-Pro-OH and Fmoc-Val-OH, and 2 × 1 h for the following amino acids). Capping of unreacted sites was performed using a mixture of acetic anhydride and DIPEA in DMF (20 min), and Fmoc deprotection was achieved by treatment with 20% piperidine in DMF (3 × 5 min). Before

DOI: 10.1021/acsomega.6b00484
ACS Omega 2017, 2, 508–516

cleaving off the linear peptide sequence, the resin was split into two batches which were kept separated over the remaining steps (be advised that the overall yield is calculated and specified only for one of the batches for each peptide). The resin was treated with 1% trifluoroacetyl (TFA) in dichloromethane (DCM, 5 × 5 min), and the resultant solutions containing the cleaved peptide were immediately neutralized with 10% pyridine in methanol. After evaporation under a steam of nitrogen, keeping approximately 5% of the initial volume, cold water was added, and the mixtures were allowed to stand in the freezer overnight. The precipitate was filtered off, washed with water, and dried under vacuum. Head-to-tail macrolactamization was performed in solution under dilute conditions.[40] A solution of the linear peptide (approximately 0.01 M) in DMF and one of HATU (1-[bis(dimethylamino)-methylene]-1*H*-1,2,3-triazolo[4,5-*b*]pyridinium 3-oxid hexafluorophosphate) (3 equiv, approximately 0.03 M) and DIPEA (6 equiv) in DMF were mixed in a round-bottomed flask by dropwise addition of the two solutions using a syringe pump. After completion, the reaction mixture was filtered through a Si-carbonate column (3 equiv relative to HATU) to remove 1-hydroxy-7-azabenzotriazole and then put on an ice bath and slowly diluted with water to get a 30:70 mixture of DMF/water. The mixture was passed through an endcapped RP-C18 column conditioned with water. The column was washed with CH_3CN/water at 30:70 to get rid of DIPEA and DMF, followed by CH_3CN/water at 85:15 to elute the peptide. The CH_3CN/water mixture was evaporated, and the resultant solid was dried under vacuum. The cyclic peptide was deprotected using a mixture of TFA/triisopropylsilane/H_2O (95:2.5:2.5). After initial cooling on an ice bath, the reaction mixture was allowed to attain room temperature. In total, the reaction mixture was stirred for 2−2.5 h and then evaporated under a nitrogen flush. Cold ether was added, and the precipitate was filtered off, washed with ether, and dried under vacuum. The crude peptide was purified using preparative HPLC.

4.1.3. Peptide **1** *c[Gly^1-Gln^2-Ser(Me)^3-Val^4-D-Pro^5-Gly^6-[3-^{13}C]Ala^7-Ser^8-Val^9-Asn^{10}].* Peptide **1** was synthesized and purified according to the general procedure described above. Importantly, the initial 300 μmol was split into two batches before cleavage from the resin and kept separated for the remaining steps (the 52% batch is reported here). The product was isolated as a white solid (62.4 mg, 46%). MS (ESI$^+$) *m*/*z*: 912.6 [M + H]$^+$. HRMS (ESI-Q-TOF) *m*/*z*: [M + H]$^+$ calcd for $C_{37}(^{13}C)H_{63}N_{12}O_{14}$, 912.4615; found, 912.4687.

4.1.4. Peptide **2** *c[Gly^1-Gln^2-Ser(Me)^3-Val^4-D-Pro^5-Gly^6-[3-^{13}C]Ala^7-Abu^8-Val^9-Asn^{10}].* Peptide **2** was synthesized and purified according to the general procedure described above. Importantly, the initial 300 μmol was split into two batches before cleavage from the resin (the 51% batch is reported here) and before macrolactamization (the 48% batch is reported here) and kept separated for the remaining steps. The product was isolated as a white solid (6.5 mg, 10%). MS (ESI$^+$) *m*/*z*: 910.7 [M + H]$^+$. HRMS (ESI-Q-TOF) *m*/*z*: [M + H]$^+$ calcd for $C_{38}(^{13}C)H_{64}N_{12}O_{13}$, 910.4823; found, 910.4748.

4.2. NMR Spectroscopy. *4.2.1. General Information.* DMSO-d_6 was used as the solvent in all experiments. Chemical shifts (δ) are reported in ppm and referenced indirectly to tetramethylsilane (TMS) via the solvent residual signal. For VT experiments, the chemical shifts (δ) are referenced to the spectrometer frequency independent of the solvent and the temperature. The NMR data was processed using the MNova software (versions 9.0 or 10.0, Mestrelab Research). Relaxation and diffusion studies were performed for the most concentrated samples to rule out peptide aggregation (data not shown).

4.2.2. One-Dimensional and Two-Dimensional NMR Data. Peptide **1** (1.0 or 1.9 mg) and peptide **2** (0.6 mg) were each dissolved in 250 μL of DMSO-d_6, and NMR spectra were recorded at 298.15 K using a 900 MHz spectrometer or at 296.15 K using a 800 MHz NMR spectrometer. $^3J_{HNH\alpha}$ coupling constants were determined using the ^{1}H NMR spectra measured on a 400 MHz NMR spectrometer. The ^{1}H NMR spectra of **1** and **2** were assigned following the sequential resonance assignment strategy combining information on scalar (J) and dipolar (NOE) connectivities obtained from total correlation spectroscopy (TOCSY) and nuclear Overhauser enhancement spectroscopy (NOESY) experiments (Tables S1 and S2).[41] Subsequently, the ^{15}N and ^{13}C NMR spectra were assigned from ^{15}N heteronuclear single quantum correlation-(HSQC) and gHSQCAD (gradient heteronuclear single quantum correlation using adiabatic sweep pulses) experiments, respectively (Tables S4 and S5). Both peptides were confirmed to adopt β-hairpin structures in DMSO-d_6 on the basis of established NMR parameters (see Supporting Information for details).

4.2.3. $^{13}C\beta$ and $^{13}C\alpha$ Structuring Shifts. For the qualitative analysis of peptides **1** and **2**, $^{13}C\beta$ and $^{13}C\alpha$ CSDs were calculated using random coil values reported for TFA-Gly^1-Gly^2-L-X^3-L-Ala^4-OCH_3 tetrapeptides (X represents one specific amino acid) dissolved in DMSO-d_6 (Tables S6 and S7, and Figures S3 and S4).[25] Reference values for non-natural amino acids were not available, and therefore CSDs could not be calculated for S(Me)3 and X8. The CSDs presented for ^{D}P5 were calculated from random coil chemical shifts for *trans* proline. Furthermore, no sequence-dependent $\delta_{random\ coil}$ values or near-neighbor correction factors are available for peptides in DMSO-d_6, which is believed to contribute to errors in the CSD analysis.

4.2.4. VT ^{13}C NMR Data—A7−$^{13}C\beta$ Detection. Peptide **1** (2 mg) and peptide **2** (2 mg) were each dissolved in 100 μL of DMSO-d_6. The NMR studies were carried out at 298.98−403.83 K, with ΔT = 4 or 5 K, using a 500 MHz spectrometer (Table S8). The two peptides were analyzed simultaneously using a spinner that can accommodate two 2.5 mm tubes.

4.2.5. VT ^{13}C NMR Data—$^{13}C\alpha$ and $^{13}C\beta$ Detection. Peptide **1** (1.9 mg) and peptide **2** (0.6 mg) were each dissolved in 250 μL of DMSO-d_6. The NMR studies were carried out at 296.15−343.15 K, with $\Delta T \approx 5$ K, using an 800 MHz spectrometer (Figures S5−S7).

4.2.6. Amide Proton Temperature Coefficients. Peptide **1** (1 mg) and peptide **2** (0.6 mg) were each dissolved in 250 μL of DMSO-d_6. Amide temperature coefficients [$\Delta\delta_{NH}/\Delta T = (\delta_{T_{high}} - \delta_{T_{low}})/(T_{high} - T_{low})$] were determined from the ^{1}H NMR spectra recorded at 338.15−363.15 K (ΔT = 5 K) using a 500 MHz spectrometer. The chemical shifts (δ) were referenced to the spectrometer frequency independent of the solvent and the temperature. Peak overlapping prohibited the determination of the coefficients for G6 and V9. Peptides (i.e., systems displaying conformational averaging) often show exceptions to the general rules for interpreting amide proton temperature coefficients.[42,43] Therefore, great caution should be taken at all interpretations. If $\Delta\delta_{NH}/\Delta T > -4$ ppb/K, there is a high probability that the amide proton is hydrogen-bonded (i.e., Q2 and A7, Tables S9 and S10). Plotting δ_{NH} against

DOI: 10.1021/acsomega.6b00484
ACS Omega 2017, 2, 508−516

temperature gave an $R^2 > 0.98$ for A7NH in **2**, and $R^2 > 0.99$ for all other amide protons.

4.2.7. NOE Buildup Analysis. Peptide **1** (1 mg) and peptide **2** (0.6 mg) were dissolved in 250 μL of DMSO-d_6. NOESY spectra were recorded at 298.15 K using a 900 MHz spectrometer. NOE buildups were recorded without solvent suppression with mixing times of 100, 200, 400, 500, 600, and 700 ms. The relaxation delay was set to 2.5 s, and 16 scans were recorded with 16 384 points in the direct dimension and 512 points in the indirect dimension. Interproton distances for protons i and j (r_{ij}) were calculated from the corresponding NOE buildup rates (σ_{ij}) and the NOE buildup rate and the interproton distance for an internal distance reference (σ_{ref} and r_{ref}), according to the equation $r_{ij} = r_{ref}(\sigma_{ref}/\sigma_{ij})^{1/6}$. Here, the geminal protons N10−Hβ1 and N10−Hβ2 were used as the reference (1.78 Å). NOE buildup rates (σ_{ij}) were determined using the normalized peak intensities [(cross peak$_i$ × cross peak$_j$)/(diagonal peak$_i$ × diagonal peak$_j$)$^{0.5}$] from the NOESY spectra at ≥5 mixing times and assuming the initial rate approximation to be valid. The data are presented in Tables S11 and S12 and in Figures S8 and S9.

4.3. CD Spectroscopy. Peptides **1** and **2** were each dissolved in CH_3CN at a concentration of ≈44 μM and transferred to 2 mm quartz cuvettes. The spectra were corrected for concentration differences. The CD spectra were recorded using a spectropolarimeter equipped with a Peltier temperature controller at 262.15−336.15 K for **1** and 260.15−342.15 K for **2**, with $\Delta T \approx 5$ K. A probe was placed inside of the cuvette to record the internal sample temperature. The VT CD data are shown in Figure 3.

4.4. Computational Conformational Analysis. Preferred low-energy conformations for **1** and **2** were generated by Monte Carlo conformational searching followed by energy minimization and clustering analysis to eliminate redundant conformations. Monte Carlo conformational searches were performed with intermediate torsion sampling, 50 000 Monte Carlo steps, and RMSD cutoff set to 2.0 Å and were followed by molecular mechanics energy minimization using the software Macromodel (v.9.1) as implemented in the Schrödinger package. Two independent conformational searches were performed using the OPLS-2005 or Amber* force fields combined with the generalized Born/surface area (GB/SA) water solvation model. Energy minimization was performed using the Polak−Ribiere-type conjugate gradient (PRCG) with maximum iteration steps set to 5000. All conformations within 42 kJ/mol from the global minimum were combined, and redundant conformations were eliminated by clustering analysis using a 2.5 Å RMSD cutoff for all heavy atom coordinates. In total, 80 and 147 conformers were identified for **1** and **2**, respectively (Table S13).

4.5. Ensemble Analysis Using the NAMFIS Software. Solution ensembles were determined by fitting the experimentally measured distances and coupling constants to those back-calculated for computationally predicted conformations following previously described protocols.[29] Dihedral angles (φ) were calculated from the experimental $^3J_{HNH\alpha}$ coupling constants using a Karplus equation calibrated to peptides.[44,45] NOE-derived distances are presented in Tables S15 and S16, whereas coupling constants are presented in Table S3. The results of the NAMFIS analysis using all experimental data are given in Table S14, the experimental output is given in Tables S15 and S16, and the conformers selected by NAMFIS are given in Figures S10 and S11. The results of the NAMFIS-analysis using only the distances and couplings involving A7 are given in Table S17, the experimental output is given in Tables S18 and S19, and the conformers selected by NAMFIS are given in Figures S12 and S13.

4.6. MD Simulations. All MD simulations were performed with GROMACS 5.1.1[46,47] using the OPLS-all atom (AA) force field.[48,49] Force field parameters for the non-natural amino acid L-2-aminobutyric acid (X8) were derived from the parameters for leucine Cβ and isoleucine Cγ. Force field parameters for the methylated serine [S(Me)3, denoted Z3 in Figure S14] were derived from serine except for the atoms of the terminal methoxy group. For the latter, the OPLS force field parameters for ethers were used (OG: opls_180, CD: opls_181, and HD1-3: opls_185). The charges for the methoxymethyl moiety (i.e., CH_2OCH_3) were changed to −0.4e for O, 0.14e for C(H_2), 0.11e for C(H_3), and 0.03e for H, according to Kahn and Bruice.[50] The parameters for the solvent DMSO were used as implemented in GROMACS 5.1.1. Initial coordinates for the backbone conformations of both peptides were taken from an output structure of the NAMFIS analysis of solution NMR data of structurally similar systems [S3 instead of S(Me)3].[18] Both peptides were solvated in a cubic box with periodic boundary conditions and a side length of 40 Å containing the peptide and approximately 440 DMSO molecules. The same MD protocol was used for both peptides. It is described in detail elsewhere.[19] Briefly, each system was equilibrated (steepest-descend minimization, 100 ps NVT, and 100 ps NPT equilibration). After that, a 100 ps MD simulation with position restraints on the peptide heavy atoms was performed, and coordinates and velocities were extracted every 10 ps. Eleven starting structures and velocities were then used to start 400 ns MD production runs (without restraints), yielding a total simulation time of 4.4 μs for each peptide. MD simulations were analyzed with a simple on/off scheme for the four backbone hydrogen bonds HB1−HB4 (Figure S14), as described previously.[19] Briefly, hydrogen bonds were detected using the Python package MDAnalysis[51] with a distance threshold of 3 Å and an angle lower limit of 120° ($\theta > 120°$). If these criteria are met, the hydrogen bond is labeled as c (closed); otherwise, it is labeled as o (open). Hydrogen bond patterns and their percentages are shown in Table S20. All hydrogen bond patterns with three or more closed backbone hydrogen bonds are defined as a folded structure; the remaining hydrogen bond patterns are defined as an unfolded structure. In the previous paper, the average hydrogen bond distance was used as the criterion, but this would result in defining cooc as folded, whereas it was defined earlier as unfolded.[19] Thus, the criterion used in this study results in a hydrogen bond pattern assignment that is consistent with the previous one. In addition to counting the occurrence of the different hydrogen bond patterns in the MD trajectories, the transition from one hydrogen bond pattern to another can be counted. This yields change maps that are shown in Tables S21 and S22.

4.7. Thermodynamic Analysis. A two-state thermodynamic equilibrium between a folded and unfolded conformational ensemble was assumed for the thermal defolding of peptides **1** and **2**.

4.7.1. VT ^{13}C NMR Data—A7–^{13}Cβ Detection. The VT ^{13}C NMR data was fitted to eq 2 by applying the Levenberg−Marquandt algorithm.[37,38] Equation 4 is derived from eqs 2 and 3, and describes the relationship between the equilibrium unfolding constants K_U and the observed and limiting chemical shifts of the folded and unfolded states (δ_{obs}, δ_F, and δ_U)

DOI: 10.1021/acsomega.6b00484
ACS Omega 2017, 2, 508−516

$$\delta_{obs} = \delta_U + \left(\frac{(\delta_F - \delta_U)}{1 + \exp\left[-\frac{\Delta H_m}{R}\left(\frac{1}{T} - \frac{1}{T_m}\right)\right]} \right) \quad (2)$$

$$K_U = \exp\left[-\frac{\Delta H_m}{R}\left(\frac{1}{T} - \frac{1}{T_m}\right)\right] \quad (3)$$

$$K_U = \frac{\delta_{obs} - \delta_F}{\delta_U - \delta_{obs}} \quad (4)$$

To evaluate the estimated limiting chemical shifts of the folded and unfolded states (δ_F and δ_U), the transition temperature T_m, and the change in enthalpy at the transition temperature, ΔH_m, Monte Carlo simulated noise was applied as a noise factor.[52] Because only part of the melting curves for **1** and **2** could be acquired, constraints were added for δ_U to improve the accuracy of the routine. From a series of calculations using rational values of δ_U (i.e., constraints) as input and 500 MC for each step, a statistical standard deviation minimum of 16.5 ± 0.5 ppm was determined for δ_U. The smallest standard deviation ranges of T_m, which were confirmed on the other parameters as well, are shown in Figures S18 and S19. To enhance the statistic deviation for each of the rational values of δ_U (i.e., constraint), the noise factor was increased. When data from linear peptides with the same sequence (data not shown) were fitted to the same equation in the same way, the results were found to agree with the cyclic peptides (i.e., δ_U = 16.5 ± 0.5 ppm). Histogram plots of δ_F, ΔH_m, and T_m, using δ_U = 16.5 ppm and 1000 MC steps, are shown in Figures S20 and S21.

In the second step, the ratio of equilibrium unfolding constants for peptide **1** (P1) and peptide **2** (P2), that is, $K_U^{P1/P2}$, for the two-state transitions is estimated from the slope of linear regression analysis of $(\delta_{obs}^{P1} - \delta_F^{P1})(\delta_U^{P2} - \delta_{obs}^{P2})$ versus $(\delta_U^{P1} - \delta_{obs}^{P1})(\delta_{obs}^{P2} - \delta_F^{P2})$. Equation 1 (vide supra) is derived from eqs 5−7 or from eqs 4 and 5.[37,38]

$$K_U^{P1/P2} = \frac{K_U^{P1}}{K_U^{P2}} = \frac{[P1_U]}{[P1_F]} \Big/ \frac{[P2_U]}{[P2_F]} = \frac{[P1_U][P2_F]}{[P1_F][P2_U]} \quad (5)$$

$$\delta_{obs}^{P1} = \frac{\delta_F^{P1}[P1_F] + \delta_U^{P1}[P1_U]}{[P1_F] + [P1_U]} \quad (6)$$

$$\delta_{obs}^{P2} = \frac{\delta_F^{P2}[P2_F] + \delta_U^{P2}[P2_U]}{[P2_F] + [P2_U]} \quad (7)$$

4.7.2. VT ^{13}C NMR Data—$^{13}C\alpha$ and $^{13}C\beta$ Detection. Shallow and partial thermal transition curves were acquired for both **1** and **2**. Representative examples are shown in Figures S22 and S23. Thus, the quality of the VT $^{13}C\alpha$ and $^{13}C\beta$ NMR data for the strand residues were not sufficient for extracting reliable limiting shifts using the curve-fitting routine, which are needed to calculate the ratio of the unfolding constants.

■ ASSOCIATED CONTENT

Supporting Information

The Supporting Information is available free of charge on the ACS Publications website at DOI: 10.1021/acsomega.6b00484.

Peptide synthesis, NMR spectroscopy, computational conformational analysis, ensemble analysis using the NAMFIS software, MD simulations, and thermodynamic analysis (PDF)

■ AUTHOR INFORMATION

Corresponding Author

*E-mail: mate@chem.gu.se (M.E.).

ORCID

Hanna Andersson: 0000-0003-3798-3322
Ashley J. Hughes: 0000-0002-9468-7442
Máté Erdélyi: 0000-0003-0359-5970

Present Addresses

[§]Hamburg Center for Ultrafast Imaging (CUI), Department of Physics, University of Hamburg, DE-22761 Hamburg, Germany (S.H.).
[‖]The Swedish NMR Centre, SE-413 96 Gothenburg, Sweden (U.B.).

Notes

The authors declare no competing financial interest.

■ ACKNOWLEDGMENTS

We thank the Swedish Research Council (#2012-3819) for the financial support. The research leading to these results has received funding from the European Research Council under the European Union's Seventh Framework Programme (FP7/2007-2013)/ERC Grant agreement no. 259638.

■ REFERENCES

(1) Mayo, K. H.; Fields, G. B. Peptides as models for understanding protein folding. In *Advances in Molecular and Cell Biology*; Bittar, E. E., Allewell, N. M., Woodward, C., Eds.; Elsevier, 1997; Vol. *22*, pp 567−612.
(2) Osterhout, J. Understanding protein folding through peptide models. *Protein Pept. Lett.* **2005**, *12*, 159−164.
(3) Waltho, J. P.; Feher, V. A.; Merutka, G.; Dyson, H. J.; Wright, P. E. Peptide models of protein folding initiation sites. 1. Secondary structure formation by peptides corresponding to the G- and H-helixes of myoglobin. *Biochemistry* **1993**, *32*, 6337−6347.
(4) Jiménez, M. A. Design of monomeric water-soluble β-hairpin and β-sheet peptides. In *Protein Design: Methods and Applications*; Köhler, V., Ed.; Springer: New York, 2014; Vol. *1216*, pp 15−52.
(5) Lewandowska, A.; Ołdziej, S.; Liwo, A.; Scheraga, H. A. β-Hairpin-forming peptides; models of early stages of protein folding. *Biophys. Chem.* **2010**, *151*, 1−9.
(6) Searle, M. S.; Williams, D. H.; Packman, L. C. A short linear peptide derived from the N-terminal sequence of ubiquitin folds into a water-stable non-native β-hairpin. *Nat. Struct. Biol.* **1995**, *2*, 999−1006.
(7) Sewald, N.; Jakubke, H.-D. Fundamental chemical and structural principles. In *Peptides: Chemistry and Biology*, 2nd ed.; Wiley-VCH: Weinheim, 2009; pp 5−61.
(8) Stotz, C. E.; Topp, E. M. Applications of model β-hairpin peptides. *J. Pharm. Sci.* **2004**, *93*, 2881−2894.
(9) Celentano, V.; Diana, D.; Di Salvo, C.; De Rosa, L.; Romanelli, A.; Fattorusso, R.; D'Andrea, L. D. 1,2,3-Triazole bridge as conformational constrain in β-hairpin peptides: Analysis of hydrogen-bonded positions. *Chem.—Eur. J.* **2016**, *22*, 5534−5537.
(10) Karnes, M. A.; Schettler, S. L.; Werner, H. M.; Kurz, A. F.; Horne, W. S.; Lengyel, G. A. Thermodynamic and structural impact of α,α-dialkylated residue incorporation in a β-hairpin peptide. *Org. Lett.* **2016**, *18*, 3902−3905.
(11) Makwana, K. M.; Mahalakshmi, R. Capping β-hairpin with N-terminal D-amino acid stabilizes peptide scaffold. *Biopolymers* **2016**, *106*, 260−266.
(12) Micsonai, A.; Wien, F.; Kernya, L.; Lee, Y.-H.; Goto, Y.; Réfrégiers, M.; Kardos, J. Accurate secondary structure prediction and

DOI: 10.1021/acsomega.6b00484
ACS Omega 2017, 2, 508−516

fold recognition for circular dichroism spectroscopy. *Proc. Natl. Acad. Sci. U.S.A.* **2015**, *112*, E3095−E3103.
(13) Shu, I.; Scian, M.; Stewart, J. M.; Kier, B. L.; Andersen, N. H. ^{13}C structuring shifts for the analysis of model β-hairpins and β-sheets in proteins: Diagnostic shifts appear only at the cross-strand H-bonded residues. *J. Biomol. NMR* **2013**, *56*, 313−329.
(14) Soth, M. J.; Nowick, J. S. A peptide/oligourea/azapeptide hybrid that adopts a hairpin turn. *J. Org. Chem.* **1999**, *64*, 276−281.
(15) Tatko, C. D.; Waters, M. L. Effect of halogenation on edge−face aromatic interactions in a β-hairpin peptide: Enhanced affinity with iodo-substituents. *Org. Lett.* **2004**, *6*, 3969−3972.
(16) Bazzo, R.; Cicero, D. O.; Barbato, G. A new 3D HCACO pulse sequence with optimized resolution and sensitivity. Application to the 21 kDa protein human interleukin-6. *J. Magn. Reson., Ser. B* **1995**, *107*, 189−191.
(17) The peptides were prepared by automated SPPS using the standard Fmoc protecting group strategy followed by head-to-tail macrolactamization in solution, side-chain deprotection and purification using preparative HPLC (Supporting Information).
(18) Danelius, E.; Brath, U.; Erdélyi, M. Insight into β-hairpin stability: Interstrand hydrogen bonding. *Synlett* **2013**, *24*, 2407−2410.
(19) Niebling, S.; Danelius, E.; Brath, U.; Westenhoff, S.; Erdélyi, M. The impact of interchain hydrogen bonding on β-hairpin stability is readily predicted by molecular dynamics simulation. *Biopolymers* **2015**, *104*, 703−706.
(20) Richardson, J. S. The anatomy and taxonomy of protein structure. In *Advances in Protein Chemistry*; Anfinsen, C. B., Edsall, J. T., Richards, F. M., Eds.; Academic Press: New York, 1981; Vol. *34*, pp 167−339.
(21) Venkatachalam, C. M. Stereochemical criteria for polypeptides and proteins. V. Conformation of a system of three linked peptide units. *Biopolymers* **1968**, *6*, 1425−1436.
(22) Kelly, S.; Price, N. The use of circular dichroism in the investigation of protein structure and function. *Curr. Protein Pept. Sci.* **2000**, *1*, 349−384.
(23) Gibbs, A. C.; Bjorndahl, T. C.; Hodges, R. S.; Wishart, D. S. Probing the structural determinants of type II′ β-turn formation in peptides and proteins. *J. Am. Chem. Soc.* **2002**, *124*, 1203−1213.
(24) Woody, R. W. Circular dichroism of peptides and proteins. In *Circular Dichroism: Principles and Applications*; Nakanishi, K., Berova, N., Woody, R. W., Eds.; VCH Publishers: New York, 1994; pp 473−496.
(25) Grathwohl, C.; Wüthrich, K. Carbon-13 NNIR of the protected tetrapeptides TFA-Gly-Gly-L-X-L-Ala-OCH$_3$, where X stands for the 20 common amino acids. *J. Magn. Reson.* **1974**, *13*, 217−225.
(26) Santiveri, C. M.; Pantoja-Uceda, D.; Rico, M.; Jiménez, M. A. β-Hairpin formation in aqueous solution and in the presence of trifluoroethanol: A ^{1}H and ^{13}C nuclear magnetic resonance conformational study of designed peptides. *Biopolymers* **2005**, *79*, 150−162.
(27) Spera, S.; Bax, A. Empirical correlation between protein backbone conformation and Cα and Cβ ^{13}C nuclear magnetic resonance chemical shifts. *J. Am. Chem. Soc.* **1991**, *113*, 5490−5492.
(28) Wishart, D. S.; Sykes, B. D.; Richards, F. M. Relationship between nuclear magnetic resonance chemical shift and protein secondary structure. *J. Mol. Biol.* **1991**, *222*, 311−333.
(29) Cicero, D. O.; Barbato, G.; Bazzo, R. NMR analysis of molecular flexibility in solution: A new method for the study of complex distributions of rapidly exchanging conformations. Application to a 13-residue peptide with an 8-residue loop. *J. Am. Chem. Soc.* **1995**, *117*, 1027−1033.
(30) Andersson, H.; Demaegdt, H.; Vauquelin, G.; Lindeberg, G.; Karlén, A.; Hallberg, M.; Erdélyi, M.; Hallberg, A. Disulfide cyclized tripeptide analogues of angiotensin IV as potent and selective inhibitors of insulin-regulated aminopeptidase (IRAP). *J. Med. Chem.* **2010**, *53*, 8059−8071.
(31) Koivisto, J. J.; Kumpulainen, E. T. T.; Koskinen, A. M. P. Conformational ensembles of flexible β-turn mimetics in DMSO-d_6. *Org. Biomol. Chem.* **2010**, *8*, 2103−2116.
(32) Erdélyi, M.; Pfeiffer, B.; Hauenstein, K.; Fohrer, J.; Gertsch, J.; Altmann, K.-H.; Carlomagno, T. Conformational preferences of natural and C3-modified epothilones in aqueous solution. *J. Med. Chem.* **2008**, *51*, 1469−1473.
(33) Jogalekar, A. S.; Damodaran, K.; Kriel, F. H.; Jung, W.-H.; Alcaraz, A. A.; Zhong, S.; Curran, D. P.; Snyder, J. P. Dictyostatin flexibility bridges conformations in solution and in the β-tubulin taxane binding site. *J. Am. Chem. Soc.* **2011**, *133*, 2427−2436.
(34) Monteagudo, E.; Cicero, D. O.; Cornett, B.; Myles, D. C.; Snyder, J. P. The conformations of discodermolide in DMSO. *J. Am. Chem. Soc.* **2001**, *123*, 6929−6930.
(35) Fridén-Saxin, M.; Seifert, T.; Hansen, L. K.; Grøtli, M.; Erdelyi, M.; Luthman, K. Proline-mediated formation of novel chroman-4-one tetrahydropyrimidines. *Tetrahedron* **2012**, *68*, 7035−7040.
(36) Mohamadi, F.; Richards, N. G. J.; Guida, W. C.; Liskamp, R.; Lipton, M.; Caufield, C.; Chang, G.; Hendrickson, T.; Still, W. C. Macromodel—an integrated software system for modeling organic and bioorganic molecules using molecular mechanics. *J. Comput. Chem.* **1990**, *11*, 440−467.
(37) Honda, S.; Kobayashi, N.; Munekata, E. Thermodynamics of a β-hairpin structure: Evidence for cooperative formation of folding nucleus. *J. Mol. Biol.* **2000**, *295*, 269−278.
(38) Honda, S.; Kobayashi, N.; Munekata, E.; Uedaira, H. Fragment reconstitution of a small protein: Folding energetics of the reconstituted immunoglobulin binding domain B1 of streptococcal protein G. *Biochemistry* **1999**, *38*, 1203−1213.
(39) Carpino, L. A.; Han, G. Y. 9-Fluorenylmethoxycarbonyl amino-protecting group. *J. Org. Chem.* **1972**, *37*, 3404−3409.
(40) Malesevic, M.; Strijowski, U.; Bächle, D.; Sewald, N. An improved method for the solution cyclization of peptides under pseudo-high dilution conditions. *J. Biotechnol.* **2004**, *112*, 73−77.
(41) Wüthrich, K. Sequential individual resonance assignments in the ^{1}H NMR spectra of polypeptides and proteins. *Biopolymers* **1983**, *22*, 131−138.
(42) Andersen, N. H.; Neidigh, J. W.; Harris, S. M.; Lee, G. M.; Liu, Z.; Tong, H. Extracting information from the temperature gradients of polypeptide NH chemical shifts. 1. The importance of conformational averaging. *J. Am. Chem. Soc.* **1997**, *119*, 8547−8561.
(43) Cierpicki, T.; Otlewski, J. Amide proton temperature coefficients as hydrogen bond indicators in proteins. *J. Biomol. NMR* **2001**, *21*, 249−261.
(44) Kessler, H.; Griesinger, C.; Lautz, J.; Mueller, A.; Van Gunsteren, W. F.; Berendsen, H. J. C. Conformational dynamics detected by nuclear magnetic resonance NOE values and J coupling constants. *J. Am. Chem. Soc.* **1988**, *110*, 3393−3396.
(45) Schmidt, J. M. A versatile component-coupling model to account for substituent effects: Application to polypeptide ϕ and χ_1 torsion related ^3J data. *J. Magn. Reson.* **2007**, *186*, 34−50.
(46) Abraham, M. J.; van der Spoel, D.; Lindahl, E.; Hess, B. *The GROMACS Development Team GROMACS User Manual*, version 5.1.1. www.gromacs.org.
(47) Pronk, S.; Pall, S.; Schulz, R.; Larsson, P.; Bjelkmar, P.; Apostolov, R.; Shirts, M. R.; Smith, J. C.; Kasson, P. M.; van der Spoel, D.; Hess, B.; Lindahl, E. GROMACS 4.5: A high-throughput and highly parallel open source molecular simulation toolkit. *Bioinformatics* **2013**, *29*, 845−854.
(48) Kaminski, G. A.; Friesner, R. A.; Tirado-Rives, J.; Jorgensen, W. L. Evaluation and reparametrization of the OPLS-AA force field for proteins via comparison with accurate quantum chemical calculations on peptides. *J. Phys. Chem. B* **2001**, *105*, 6474−6487.
(49) Rizzo, R. C.; Jorgensen, W. L. OPLS all-atom model for amines: Resolution of the amine hydration problem. *J. Am. Chem. Soc.* **1999**, *121*, 4827−4836.
(50) Kahn, K.; Bruice, T. C. Parameterization of OPLS-AA force field for the conformational analysis of macrocyclic polyketides. *J. Comput. Chem.* **2002**, *23*, 977−996.
(51) Michaud-Agrawal, N.; Denning, E. J.; Woolf, T. B.; Beckstein, O. MDAnalysis: A toolkit for the analysis of molecular dynamics simulations. *J. Comput. Chem.* **2011**, *32*, 2319−2327.

DOI: 10.1021/acsomega.6b00484
ACS Omega 2017, 2, 508−516

(52) Alper, J. S.; Gelb, R. I. Standard errors and confidence intervals in nonlinear regression: Comparison of Monte Carlo and parametric statistics. *J. Phys. Chem.* **1990**, *94*, 4747−4751.

DOI: 10.1021/acsomega.6b00484
ACS Omega 2017, 2, 508−516